

EXPERIMENTAL TEST OF LONGITUDINAL SPACE-CHARGE AMPLIFIER IN OPTICAL RANGE

C. Lechner*, M. Dohlus, B. Faatz, V. Grattoni, G. Paraskaki, J. Rösensch-Schulenburg, E. Schneidmiller, M. Yurkov, J. Zemella, DESY, 22607 Hamburg, Germany
V. Miltchev, University of Hamburg, 22761 Hamburg, Germany

Abstract

Longitudinal space-charge effects can act as a driver for short wavelength radiation production in a longitudinal space-charge amplifier (LSCA). A single cascade of an LSCA was tested using the hardware of the sFLASH experiment installed at the FEL user facility FLASH (at DESY, Hamburg). Scans of the longitudinal dispersion of the chicane were performed with the tightly focused electron beam for different compression settings, while recording the intensity of the emission from a few-period undulator. We present experimental results and estimates on electron beam properties.

INTRODUCTION

Longitudinal space-charge (LSC) effects are a driver of the so-called microbunching instability (MBI) that can compromise the quality of the high-brightness electron bunches driving modern free-electron lasers (FELs). Unless mitigated by a laser heater, this instability affects the operating of these devices as well as the performance of the FEL process itself [1–6]. The longitudinal space-charge amplifier (LSCA) [7] exploits LSC effects for the generation of bunching (and radiation when injected into an undulator) at short wavelengths. An LSCA is a sequence of amplification cascades, each one comprising an electron beamline and a dedicated chicane. In the beamline, higher-current regions expand longitudinally due to LSC forces. The resulting energy deviations are then converted into density modulations by the longitudinal dispersion of the chicane. Starting from shot noise, a strong density modulation can be obtained after typically two to four cascades.

At SLAC's Next Linear Collider Test Accelerator (NLCTA), the impact of compression changes on a three-stage LSCA starting from shot noise was studied experimentally [8]. Longitudinal phase-space distributions affected by MBI were studied at LCLS using an RF deflector [9]. Finally, a microbunching gain process can also be initiated in a controlled way by generating the electron bunch using an injector laser with a modulated laser pulse [10] or by manipulating the electron bunch further downstream in the machine [11].

In this contribution, we report on recent experiments at the FEL user facility FLASH at DESY, Hamburg [12]. High-brightness electron bunches arriving from the energy collimator (dogleg) of FLASH1 were transported along a beamline operated with the electron optics specifically designed for small transverse beam extent. In a subsequent chicane

with variable longitudinal dispersion R_{56} , the beam was manipulated and the visible emission from a few-period undulator was recorded. This signal enables us to diagnose longitudinal density modulations in the electron beam and to infer on its slice energy spread.

EXPERIMENTAL LAYOUT

The schematic layout of the FEL user facility FLASH is shown in Fig. 1. The superconducting linear accelerator (linac) driving the FEL delivers high-brightness electron bunches with energies up to 1.25 GeV. At a repetition rate of 10 Hz, bunch trains consisting of up to 800 bunches at a 1-MHz repetition rate can be produced. These bunch trains are distributed over the undulator beamlines FLASH1 and FLASH2 with a flat-top kicker and a Lambertson DC septum, enabling full 10-Hz repetition rate operation of both beamlines.

For these measurements, hardware of the sFLASH seeding experiment [13] was used. It is installed in the FLASH1 electron beamline between the energy collimation section (dogleg) and the FLASH1 undulator system, compare Fig. 2. The electron bunches arriving from the dogleg are transported along a beamline section in which LSC effects can act on the beam and then through a four-dipole chicane with variable longitudinal dispersion. Eventually, the electron bunch is transported through an electromagnetic undulator (5 periods of $\lambda_u = 20$ cm, $K_{\max} = 10.8$). As the electron bunch traverses the undulator, light pulses in the visible wavelength range are generated that are extracted from the beamline by a metallic OTR screen and are recorded by a camera (the electron bunch is guided around the OTR screen by another small chicane). For the measurements in this paper, a bandpass filter with a central wavelength of 535 nm and a bandwidth of 45 nm was inserted into the optical beamline. Finally, to obtain information about the electron bunches, the longitudinal phase-space distribution was mapped out in a combination of transverse-deflecting structure (TDS), an RF deflector introducing a longitudinal-to-vertical correlation, and a dipole spectrometer. This enabled us to obtain the peak current for the different compression settings under study.

RESULTS

Electron bunches with a charge of 0.14 nC, a beam energy of 748 MeV, and different compression states were transported through an approx. 4-m-long channel operated with a dedicated optics putting emphasis on minimized transverse extent. After this section in which LSC effects can act on the

* christoph.lechner@desy.de

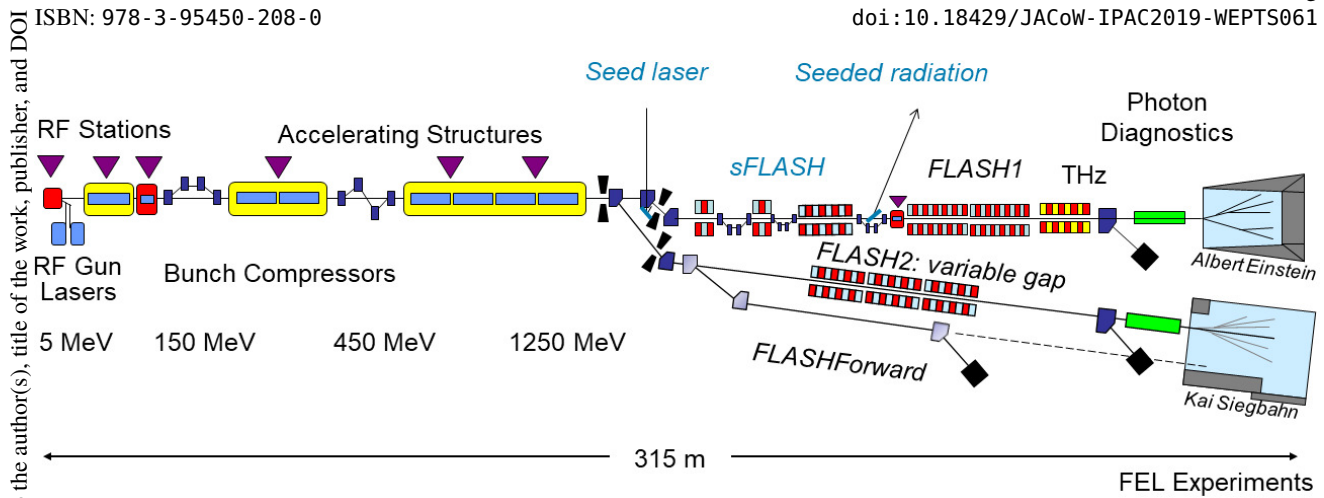


Figure 1: Schematic layout of FLASH user facility. The experiment was performed using the hardware of the seeding experiment sFLASH which is installed in the FLASH1 undulator beamline.

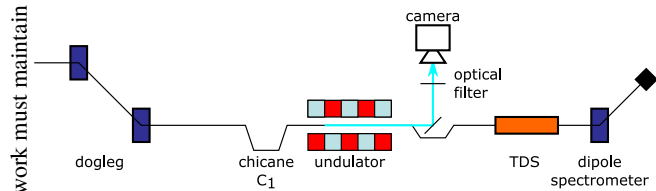


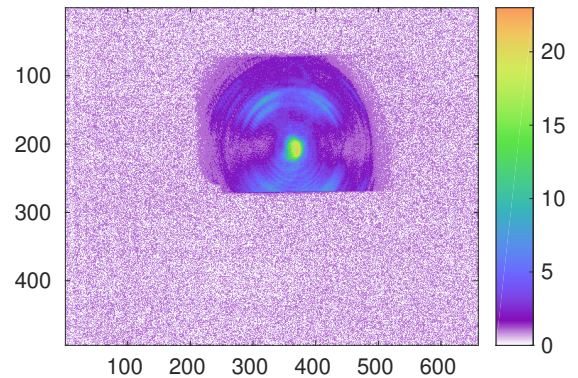
Figure 2: Schematic layout of the experiment. The electron bunches arriving from the dogleg are transported along an approx. 4-m-long beamline segment. After chicane C_1 , the emission from a five-period undulator is extracted from the beamline by an OTR screen and sent to the camera station. The longitudinal phase-space distribution of the bunches can be measured in a combination of transverse-deflecting structure (TDS) and dipole spectrometer.

beam, a four-dipole chicane with variable longitudinal dispersion manipulates the electron beam, interrelating energy deviations and longitudinal density modulations. Following this dispersive section, a five-period undulator was used as a diagnostic device. With the bandpass filter inserted in front of the camera, the undulator was tuned to a wavelength $\lambda = 610$ nm, which optimized the spatial profile of the emitted undulator radiation to a round spot.

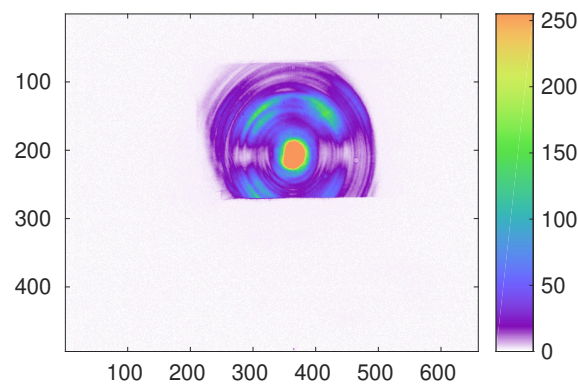
The acquired raw camera images were first corrected for the dark signal and then sum-of-pixels values were computed over the sensor area illuminated by the emission from the undulator. For illustration, Fig. 3 shows two raw images from a scan with bunches compressed to 0.4-kA peak current that were acquired at longitudinal dispersions with minimum and maximum signal, respectively.

For each step of the longitudinal dispersion scan, 30 consecutive images were selected and the average signal and the signal's standard deviation, which indicates shot-to-shot fluctuations, were computed. The obtained values are indicated in Figs. 4 and 5.

The scan conducted with 0.4-kA peak current electron bunches is shown in Fig. 4. A clear signal reduction can be observed in this case with an integrated signal about 40 %



(a) Minimum signal



(b) Maximum signal

Figure 3: Example images obtained for longitudinal dispersions giving minimum and maximum signal in the 0.4-kA scan shown in Fig. 4. Note the different color coding in the panels.

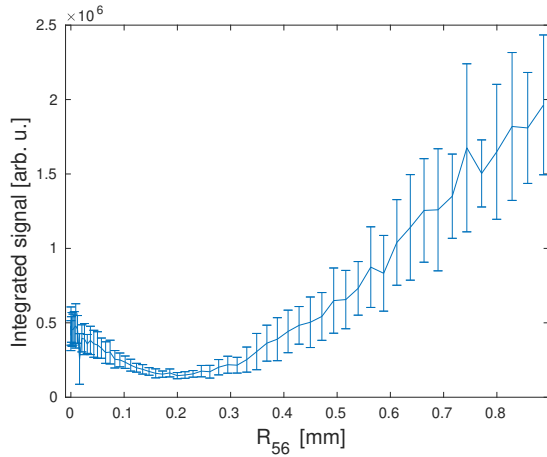


Figure 4: Scan of the longitudinal dispersion R_{56} with a peak current of 0.4 kA.

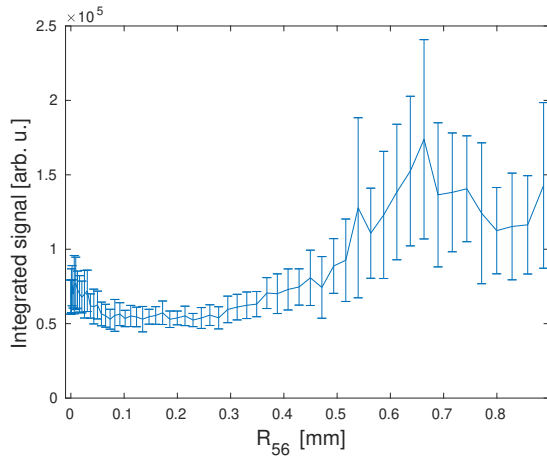


Figure 5: Scan of the longitudinal dispersion R_{56} with a peak current of 1.0 kA.

of its value when the chicane is off. We note that in the data from which Fig. 4 was prepared the undulator emission partially saturated the camera for R_{56} below 0.09 mm and R_{56} above 0.34 mm (see Fig. 3b for an example image). This saturation effect leads to an underestimation of the integrated signal for small longitudinal dispersions, which may in turn result in an underestimation of the observed signal reduction. The signal reduction seen in Fig. 4 around $R_{56} \approx 0.20$ mm can be interpreted as the shot noise suppression effect [14] previously observed at LCLS [15]. Another feature to be expected in an R_{56} scan is a maximum that is defined by the uncorrelated energy spread. From the gain formula for a single cascade of LSCA [7], one can obtain the position of the maximum:

$$R_{56} \approx \frac{\lambda\gamma}{2\pi\sigma_\gamma}. \quad (1)$$

here, λ is the wavelength, γ is the relativistic factor, and σ_γ is the rms uncorrelated energy spread (in units of rest energy). For the 0.4-kA beam, the optimum R_{56} value is outside of the accessible range. Therefore, we also performed scans

with a stronger beam compression. In Fig. 5, scan results obtained for a beam current of 1.0 kA can be seen. From Eq. 1 we can estimate the uncorrelated energy spread to be (94 ± 18) keV. This value is in the expected range for a 1-kA beam according to start-to-end simulations [16, 17]. We can conclude that our simple setup can be used for quick measurements of uncorrelated energy spread at FLASH in the future.

SUMMARY AND OUTLOOK

We tested a single cascade of LSCA in the optical wavelength range, and observed both gain and noise suppression. We demonstrated that this simple setup can be used to extract information about the uncorrelated energy spread of compressed electron bunches at FLASH. A hardware upgrade of the chicane that was used to manipulate the electron beam with variable R_{56} is currently being prepared. After installation, the extended longitudinal dispersion range will enable measuring the uncorrelated energy spread of electron bunches at lower peak current. Additionally, a Ce:YAG screen capable to diagnose the on-axis undulator radiation while a chicane guides the electron beam around the screen would enable studies of LSCA gain at shorter wavelengths.

ACKNOWLEDGEMENTS

We thank DESY and the FLASH team for the opportunity to perform our experiment.

REFERENCES

- [1] H. Loos *et al.*, “Observation of Coherent Optical Transition Radiation in the LCLS Linac”, in *Proc. 30th Int. Free Electron Laser Conf. (FEL’08)*, Gyeongju, Korea, Aug. 2008, paper THBAU01, pp. 485–489.
- [2] S. Wesch, C. Behrens, B. Schmidt, and P. Schmüser, “Observation of Coherent Optical Transition Radiation and Evidence for Microbunching in Magnetic Chicanes”, in *Proc. 31st Int. Free Electron Laser Conf. (FEL’09)*, Liverpool, UK, Aug. 2009, paper WEPC50, pp. 619–622.
- [3] C. Behrens *et al.*, “Electron beam profile imaging in the presence of coherent optical radiation effects”, *Phys. Rev. ST Accel. Beams* 15, 062801 (2012). doi:10.1103/PhysRevSTAB.15.062801
- [4] S. Matsubara *et al.*, “Improvement of Screen Monitor with Suppression of Coherent-OTR Effect for SACLA”, in *Proc. 1st Int. Beam Instrumentation Conf. (IBIC’12)*, Tsukuba, Japan, Oct. 2012, paper MOCC04, pp. 34–37.
- [5] Z. Huang *et al.*, “Measurements of the linac coherent light source laser heater and its impact on the x-ray free-electron laser performance”, *Phys. Rev. ST Accel. Beams* 13, 020703 (2010). doi:10.1103/PhysRevSTAB.13.020703
- [6] S. Spampinati *et al.*, “Commissioning of the FERMI@ELETTRA Laser Heater”, in *Proc. 34th Int. Free Electron Laser Conf. (FEL’12)*, Nara, Japan, Aug. 2012, paper MOPD58, pp. 177–180.
- [7] E.A. Schneidmiller and M.V. Yurkov, “Using the longitudinal space charge instability for generation of vacuum ultraviolet

- and x-ray radiation”, *Phys. Rev. ST Accel. Beams* 13, 110701 (2010). doi:10.1103/PhysRevSTAB.13.110701
- [8] A. Marinelli *et al.*, “Generation of Coherent Broadband Photon Pulses with a Cascaded Longitudinal Space-Charge Amplifier”, *Phys. Rev. Lett.* 110, 264802 (2013). doi:10.1103/PhysRevLett.110.264802
- [9] D. Ratner *et al.*, “Time-resolved imaging of the microbunching instability and energy spread at the Linac Coherent Light Source”, *Phys. Rev. ST Accel. Beams* 18, 030704 (2015). doi:10.1103/PhysRevSTAB.18.030704
- [10] S. Seletskiy *et al.*, “Seeding, Controlling, and Benefiting from the Microbunching Instability”, *Phys. Rev. Lett.* 111, 034803 (2013). doi:10.1103/PhysRevLett.111.034803
- [11] E. Roussel *et al.*, “Multicolor High-Gain Free-Electron Laser Driven by Seeded Microbunching Instability”, *Phys. Rev. Lett.* 115, 214801 (2015). doi:10.1103/PhysRevLett.115.214801
- [12] J. Rönisch-Schulenburg *et al.*, “Status of the Superconducting Soft X-Ray Free-Electron Laser User Facility Flash at DESY”, presented at the *10th Int. Particle Accelerator Conf. (IPAC'19)*, Melbourne, Australia, May 2019, paper TUPRB106, this conference.
- [13] C. Lechner *et al.*, “Status of the sFLASH Experiment”, in *Proc. 9th Int. Particle Accelerator Conf. (IPAC'18)*, Vancouver, Canada, Apr.-May 2018, pp. 1471–1473. doi:10.18429/JACoW-IPAC2018-TUPMF085
- [14] A. Gover and E. Dyunin, “Collective-Interaction Control and Reduction of Optical Frequency Shot Noise in Charged-Particle Beams”, *Phys. Rev. Lett.* 102, 154801 (2009). doi:10.1103/PhysRevLett.102.154801
- [15] D. Ratner and G. Stupakov, “Observation of Shot Noise Suppression at Optical Wavelengths in a Relativistic Electron Beam”, *Phys. Rev. Lett.* 109, 034801 (2012). doi:10.1103/PhysRevLett.109.034801
- [16] I. Zagorodnov and M. Dohlus, “Beam Dynamics and FEL Simulations for FLASH”, online: http://www.desy.de/fel-beam/s2e/flash/Nominal/flashI/IZ_2010_February.pdf, last access: 30.04.2019.
- [17] G. Feng *et al.*, “Start-to-End Simulation for FLASH2 HGHG Option”, in *Proc. 36th Int. Free Electron Laser Conf. (FEL'14)*, Basel, Switzerland, Aug. 2014, paper MOP083, pp. 244–247.